Hindawi
Geofluids
Volume 2021, Article ID 6674616, 10 pages
https://doi.org/10.1155/2021/6674616

Research Article

Surrounding Rock Failure Characteristics and Water Inrush Mechanism of Roadway above the Aquifer in Nonuniform Stress Field

Xiaofei Guo,[1] **Yongen Li**,[1,2] **Jun Li**,[1] **Hongyu Liu**,[1] **Xianjie Ma**,[1] **Ji Li**,[3] **Guoyu Li**,[4] **and Jihao Tan**[4]

[1]*School of Energy and Mining Engineering, China University of Mining and Technology, Beijing 100083, China*
[2]*China Energy Guoyuan Electric Power Group, Beijing 100033, China*
[3]*School of Energy, Xi'an University of Science and Technology, Xi'an 710054, China*
[4]*Longmenxia South Coal Mine of Sichuan Huayingshan Coal Industry Co., Ltd., Guang'an 638020, China*

Correspondence should be addressed to Yongen Li; leeynai@126.com

Received 17 November 2020; Revised 11 January 2021; Accepted 13 January 2021; Published 29 January 2021

Academic Editor: Yanlin Zhao

The expansion of the roadway surrounding rock failure zone may connect the floor aquifer and cause the roadway water inrush. In order to reveal the mechanism of the roadway water inrush above confined water, we established the force model of the roadway surrounding rock above confined water in nonuniform stress field and studied the shape characteristics and expansion law of the roadway surrounding rock plastic zone. The results show that the roadway surrounding rock will form three kinds of plastic zone under different lateral pressure coefficients: circular, elliptical, and butterfly; when the shape of plastic zone is circular or elliptic, the maximum radius increases linearly with the increase of regional stress; when the shape is butterfly, the maximum radius increases exponentially with the increase of stress. Under the condition of a larger bidirectional stress ratio, the surrounding rock of the roadway will show butterfly-shaped failure, and small stress change will cause malignant expansion of the plastic zone; when the plastic zone is connected with the underlying aquifer, confined water of floor will enter the rock mass from the water diversion point and eventually flood into the roadway, causing floor water inrush.

1. Introduction

The rescue of coal mine water inrush accident is difficult, and it takes a long time for the mine to resume normal production, which often causes huge economic losses and casualties [1–3]. With the increasing of mining depth and intensity, the hydrogeological conditions of coalfield are becoming more and more complex, and the threat of floor confined water to mine safety production is increasingly serious [4–6].

At present, many researchers have made some innovative explorations on the mechanism of floor water inrush. As the working face of coal mining continues to advance, joints and cracks in the floor will develop continuously until the underlying confined water and the upper part are connected through cracks [7–10]. Liu et al. carried out numerical simulation of water inrush caused by fault lag [11]. Cheng et al. carried out numerical simulation of fault activation process considering fluid solid coupling [12]. Wu et al. [13–15] found that FLAC software is an effective tool for simulation and evaluation of water inrush prevention capacity of coal seam floor, and they discussed the law of delayed water inrush when coal seam floor contains fracture structure. Some scholars have gradually realized that the fracture propagation and failure of floor rock mass under the influence of mining are closely related to the macro and micro structural characteristics [16–19]. Yin [20] supposed that water inrush channel played a key role in floor water inrush, so he puts forward the concept of "strong seepage channel". Zhao et al. [21–23] studied the flow law of water in fractures and further proved that fractures or damaged areas were the channels of underground water inrush. It can be seen that the surrounding rock failure area is an important water

diversion channel during water inrush. However, the process and mechanism of conducting confined water due to the expansion of surrounding rock failure zone are still insufficient. This study will focus on the development process of the surrounding rock failure zone after mining and then reveal the formation mechanism of the water channel.

Since the floor roadway is dug under the coal seam, the mining of the upper coal seam will form a nonuniform stress field around the roadway [24–26]. Under the influence of mining stress field, the surrounding rock of roadway will form a certain range of failure zones, and the failure range of surrounding rock of floor roadway directly determines the size of water inrush risk of coal seam and floor roadway [27–30]. In order to reveal the mechanism of water inrush of roadway above confined water, the force model of the roadway surrounding rock above confined water in nonuniform stress field was established, and the failure law of surrounding rock in nonuniform stress field after roadway excavation was studied, and the mechanism of water flowing fracture zone formed by expansion of surrounding rock failure zone in nonuniform stress field was explained.

2. Surrounding Rock Failure Characteristics of Roadway above Confined Water in Nonuniform Stress Field

2.1. Force Model. When confined water exists in the floor rock of roadway, the surrounding rock failure zone of roadway may connect the aquifer, causing water inrush risk. The aquiclude is located between the rock layer and the aquifer. The aquifer under the aquiclude is composed of skeleton and confined water filled with aquifer cracks. According to hydrogeology, the weight of the overlying strata in an aquifer is borne by both the skeleton in the aquifer and the confined water in the aquifer. When the hydrostatic pressure of aquifer remains constant, the change of overlying load will cause the change of aquifer skeleton stress. The hydrostatic pressure of confined water in aquifer provides support to the aquiclude of roadway floor, forming an additional stress field in the floor aquiclude [27]. According to hydrogeology, the vertical stress P_Z generated above the study area will make the skeleton of the aquifer below produce corresponding force P_Z, and the existence of water pressure P_W below will also make the upper boundary of the study area produce the same size and opposite direction reaction force. Therefore, the plane strain model of circular hole is established as follows: the internal geometric boundary is a circular hole with radius of r_0; P_X and P_Z are the horizontal and vertical stresses of regional stress field under the original rock stress state; λ is the lateral pressure coefficient, and $P_X = \lambda \times P_Z$; P_W is the hydrostatic pressure of water pressure on the upper aquiclude. Finally, the surrounding rock mechanical model of circular roadway above confined water in nonuniform stress field is established, as shown in Figure 1.

Based on Mohr Coulomb strength criterion, Li et al. [29] established the implicit plastic boundary equation of the surrounding rock of circular roadway under the influence of water pressure under two-way nonuniform pressure stress field, as shown in the following:

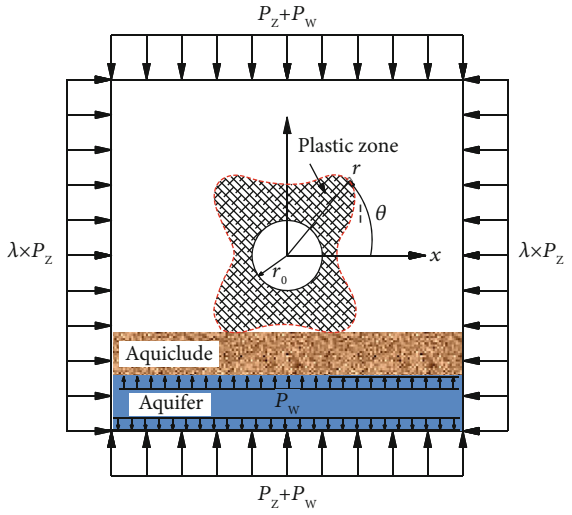

Figure 1: Surrounding rock force model of circular roadway in nonuniform stress field under the influence of water pressure.

$$
\begin{aligned}
&9(1-\lambda)^2\left(\frac{r_0}{r}\right)^8+\left[-12(1-\lambda)^2+6\left(1-\lambda^2\right)\cos 2\theta\right]\left(\frac{r_0}{r}\right)^6\\
&+\begin{bmatrix}10(1-\lambda)^2\cos^2 2\theta-4(1-\lambda)^2\sin^2\varphi\cos^2 2\theta\\ -2(1-\lambda)^2\sin^2 2\theta-4\left(1-\lambda^2\right)\cos 2\theta+(1+\lambda)^2\end{bmatrix}\left(\frac{r_0}{r}\right)^4\\
&+\begin{Bmatrix}-4(1-\lambda)^2\cos 4\theta+\left[2-2\lambda^2-4\left(1-\lambda^2\right)\sin^2\varphi\right]\cos 2\theta\\ -\dfrac{[4C[(\lambda\text{-}1)\gamma H+(\lambda\text{-}1)P_w]\sin 2\varphi\cos 2\theta]}{(\lambda\gamma H+\lambda P_w)^2}\end{Bmatrix}\left(\frac{r_0}{r}\right)^2\\
&+\left[(1-\lambda)^2-\sin^2\varphi\left(1+\lambda+\frac{2C\cos\varphi}{\lambda(\gamma H+P_w)\sin\varphi}\right)^2\right]=0.
\end{aligned}
\tag{1}
$$

When the vertical load P_Z, lateral pressure coefficient λ, water pressure P_W, roadway radius r_0, surrounding rock cohesion C, and surrounding rock internal friction angle φ are determined, the boundary range of plastic zone of surrounding rock of circular roadway can be calculated.

2.2. Shape Characteristics of the Roadway Plastic Zone in Nonuniform Stress Field. The stress field in formula (1) mainly includes vertical load P_Z, lateral pressure coefficient λ, and floor water pressure P_W. Among them, the water pressure P_W of the aquifer is a relatively stable, which tends to increase with the increase of buried depth, and is relatively stable under certain geological conditions. In the deep underground conditions, although the surrounding rock stress field is complex, its vertical stress P_Z is basically equal to the unit weight of overlying strata γH, and the horizontal stress is usually greater than the vertical stress under the influence of geological structure in the original rock state. Under the influence of different geological structures and mining stress, the horizontal stress and vertical stress will also be different, which will lead to the large variation of lateral pressure coefficient. The coefficient of lateral pressure represents the ratio

of horizontal stress to vertical stress, reflects the difference between horizontal stress and vertical stress, and represents the nonuniformity of stress field. According to the geological conditions of floor roadway in Zhaogu No. 2 mine ($H = 700$ m, $r_0 = 2.5$ m, $C = 3$ MPa, $\varphi = 25°$), fixed $P_Z = \gamma H = 17.5$ MPa, this study calculates the plastic zone when lateral pressure coefficient λ is 1, 2, 2.5, and 3 ($P_X = 21.5$ MPa, 35 MPa, 43.75 MPa, and 52.5 MPa), as shown in Figure 2.

When $\lambda = 1$, the boundary of plastic zone of surrounding rock is circular, and the failure depth of plastic zone is 0.45 m. With the increase of lateral pressure coefficient, the boundary shape of plastic zone of roadway surrounding rock changed from circular to ellipse with a long axis on the y-axis and a minor axis on the x-axis, and the maximum failure range increased to 1.27 m. When $\lambda = 2.5$, the boundary of plastic zone of surrounding rock of roadway is sunken in the direction of principal stress and protrudes on the bisector of two principal stresses. At this time, the plastic failure range of surrounding rock is increased to 2.61 m. Because the distribution of plastic zone is similar to a butterfly, the plastic zone with nonuniform distribution is defined as a butterfly-shaped plastic zone. At this time, there are four maximum boundaries and four minimum boundaries in the plastic zone, and the plastic zone in the direction of maximum boundary is defined as "butterfly leaf." When $\lambda = 3$, the boundary of plastic zone presents obvious "butterfly" distribution characteristics, and the maximum failure range increases obviously, reaching 5.63 m. It can be seen that with the increase of the lateral pressure coefficient, the shape of the plastic zone of the roadway surrounding rock presents obvious change characteristics from circular to elliptic to butterfly shaped.

2.3. The Influence of Lateral Pressure Coefficient on the Roadway Plastic Zone. According to the geological conditions of floor roadway in Zhaogu No. 2 Coal Mine, the lateral pressure coefficient ($\lambda = 1$, $\lambda = 1.5$, and $\lambda = 3$) is fixed to make the plastic zone in different shape characteristics. The statistical results of the maximum radius R_{max} of the plastic zone are obtained by changing the horizontal stress, as shown in Figure 3. In Figure 3, the R_{max} of the butterfly shape uses the primary axis, while the R_{max} of the circular or elliptic shape uses the secondary axis. When the shape of plastic zone is circular or ellipse, the maximum radius of plastic zone increases linearly with the increase of regional stress; when the shape of plastic zone is butterfly shaped, the maximum radius of plastic zone increases exponentially with the increase of regional stress, and when the principal stress reaches a certain limit value ($P_X = 43.5$ MPa, $\lambda = 3$), the maximum radius of plastic zone tends to infinity. It shows that the plastic zone will expand rapidly with the increase of the principal stress when shape of plastic zone is butterfly but that no matter how large the stress is, the plastic zone does not expand rapidly in the circular and elliptical shapes. The characteristics of rapid expansion show that the size of plastic zone is very sensitive when it is butterfly shaped. Under high lateral pressure coefficient, the slight change of regional principal stress will cause the malignant expansion of butterfly shaped plastic zone. After a butterfly-shaped plastic zone appears in the surrounding rock, a small change of regional stress will cause malignant expansion of the butterfly-shaped plastic zone.

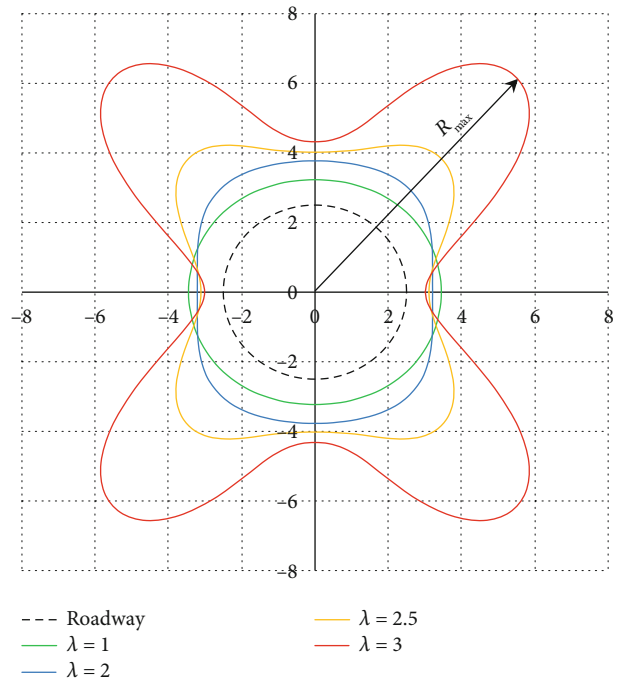

Figure 2: Characteristics of surrounding rock plastic zone under different lateral pressure coefficient: $P_W = 4$ MPa, $r_0 = 2.5$ m, $C = 3$ MPa, and $\varphi = 25°$.

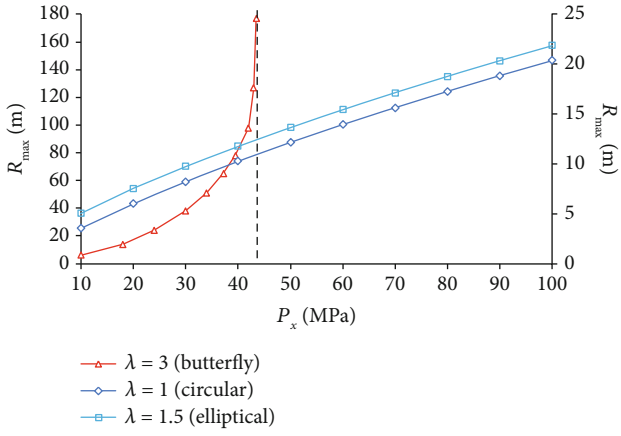

Figure 3: The relationship between the radius of the plastic zone and stress under different plastic zone shapes.

Based on the geological conditions of the floor roadway in Zhaogu No. 2 Coal Mine, the vertical stress and water pressure ($P_Z = 17.5$ MPa, $P_W = 4$ MPa) are fixed. By increasing and decreasing the horizontal stress, the R_{max} under different lateral pressure coefficients are obtained, as shown in Figure 4.

It can be seen from Figure 4 that R_{max} gradually increases with the increase of λ when $\lambda > 1$. When $\lambda = 2.306$, the shape of plastic zone is the critical point of elliptic transformation into a butterfly shape. Therefore, when $1 < \lambda < 2.306$, R_{max}

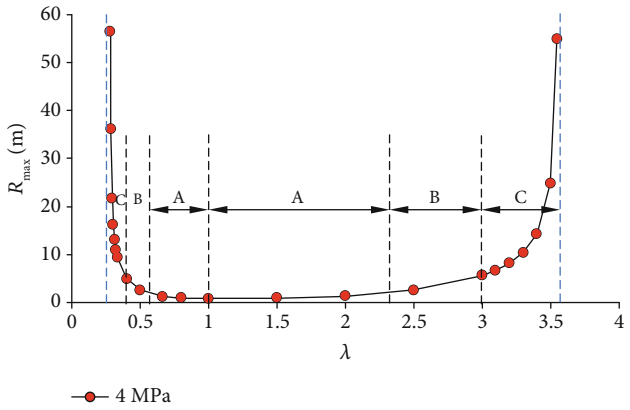

Figure 4: Complete stress ratio curve.

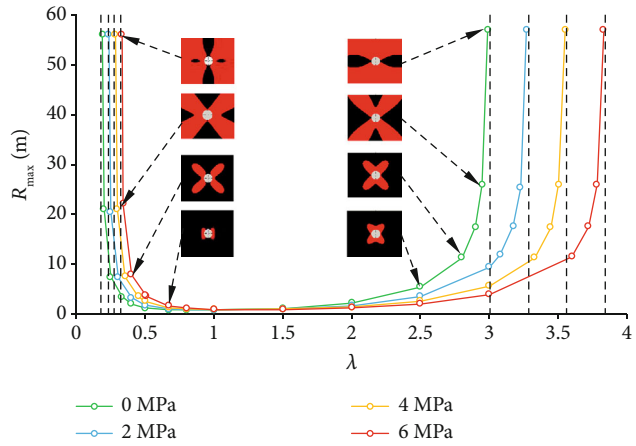

Figure 5: The relationship between radius of the plastic zone and stress under the different water pressure.

increases slowly with the increase of λ. When $\lambda > 2.306$, the expansion size of plastic zone is still controllable in the early stage of butterfly shape. When $\lambda = 3$, R_{max} is twice the radius of the roadway. When $\lambda > 3$, the slight change of stress will lead to the exponential growth of R_{max}.

When $\lambda < 1$, that is, the horizontal stress is less than the vertical stress; with the decrease of λ, the increasing trend of R_{max} is similar to that of $\lambda > 1$. At this time, when $\lambda = 0.53$, the shape of plastic zone is at the critical point of transforming from ellipse to butterfly shape. When $\lambda < 0.53$, R_{max} increases slowly with the decrease of λ. When $\lambda < 0.53$, the plastic zone becomes butterfly shape, and the size of plastic zone increases exponentially with the decrease of λ. When $\lambda = 0.4$, R_{max} reaches 2 times of roadway radius. When $\lambda < 0.4$, the ratio of R_{max} growth to stress presents high sensitivity, and the small change of λ will lead to rapid growth of R_{max}.

With the increase of the lateral pressure coefficient ($\lambda > 1$) or decrease ($\lambda < 1$), the shape of the plastic zone changes from circular to ellipse. When $1 < \lambda < 2.306$ or $0.53 < \lambda < 1$, R_{max} in the area shows a linear slow growth trend, which is called the linear slow growth area, as shown in the area A of the figure. When $2.306 < \lambda < 3$ or $0.4 < \lambda < 0.53$, the plastic zone becomes butterfly shape, and the plastic zone expansion size is less than 2 times of roadway radius; this area is defined as a butterfly controllable area, as shown in area B in the figure. When $\lambda > 3$ or $\lambda < 0.4$, the slight change of stress will lead to the malignant rapid growth of R_{max}. This region is defined as a butterfly-shaped malignant growth area, as shown in area C in the figure.

2.4. The Influence of Water Pressure on the Roadway Plastic Zone. The water pressure in the aquifer can be seen as an additional stress field acting on the aquiclude before water in the aquifer flow into the extracted space. And the water pressure in the aquifer is also different under different buried depths. Taking Zhaogu No. 2 Coal Mine as an example, the water pressure in the aquifer is 3.24~6.84 MPa. According to the geological conditions of floor roadway in Zhaogu No. 2 Coal Mine, the maximum radius R_{max} of plastic zone of surrounding rock under different water pressure conditions (0 MPa, 2 MPa, 4 MPa, and 6 MPa) and different stress ratios is calculated, as shown in Figure 5.

It can be seen that when $\lambda > 1$, that is, the horizontal stress is greater than the vertical stress; the plastic zone expansion characteristics of surrounding rock are the same under different water pressure conditions. With the increase of λ, the shape of plastic zone presents the characteristics of circular ⟶ elliptic ⟶ butterfly shaped, and the growth trend of plastic zone size is linear growth ⟶ controllable growth ⟶ malignant growth. The limit stress ratio λ_{max} of surrounding rock is different under different water pressure. When the water pressure is 0 MPa, 2 MPa, 4 MPa, and 6 MPa, the corresponding limit stress ratio is 2.99, 3.2706, 3.551, and 3.782, respectively. When $\lambda = 3$, the R_{max} values of 0 MPa, 2 MPa, 4 MPa, and 6 MPa are ∞, 9.39 m, 5.63 m, and 3.94 m, respectively. It can be seen that when $\lambda > 1$, the limit stress ratio λ_{max} under different water pressure conditions increases gradually with the increase of water pressure. Under the same stress ratio condition, the greater the water pressure, the smaller the maximum radius R_{max} of plastic zone. Therefore, when the horizontal stress is greater than the vertical stress, the water pressure can restrain the expansion of the plastic zone.

When $\lambda < 1$, that is, the horizontal stress is less than the vertical stress, the expansion characteristics of plastic zone of surrounding rock are the same, and the limit stress ratio λ_{max} of surrounding rock under different water pressure is also different. When the water pressure is 0 MPa, 2 MPa, 4 MPa, and 6 MPa, the corresponding limit stress ratios are 0.1895, 0.236, 0.2826, and 0.3292, respectively. When $\lambda = 0.5$, the R_{max} values of 0 MPa, 2 MPa, 4 MPa, and 6 MPa are 1.18 m, 1.74 m, 2.58 m, and 3.74 m, respectively. When $\lambda < 1$, the limit stress ratio will increase with the increase of water pressure. Under the same stress ratio condition, the greater the water pressure, the greater the maximum radius R_{max} of plastic zone is. Therefore, when the horizontal stress is less than the vertical stress, the water pressure promotes the expansion of the surrounding rock plastic zone around the floor roadway.

3. Numerical Simulation Verification

The above research contents are all conclusions obtained under homogeneous media conditions. In fact, the surrounding rock

of roadway in an underground mine is often stratified, and the properties of each rock strata are very different. The content of this section is built on the actual engineering conditions of the Zhaogu No. 2 Coal Mine, using FLAC^{3D} numerical simulation software to study the failure characteristics of the roadway surrounding rock in the layered medium conditions. Furthermore, the water inrush mechanism of the roadway surrounding rock in the nonuniform stress field is revealed.

3.1. Case Engineering Background. Zhaogu No. 2 Coal Mine is a newly built mine of Jiaozuo Coal Industry Group. The main coal seam is 2-1 coal seam with a thickness of 6.0 m to 6.59 m, which is a high gas mine. In order to effectively eliminate the risk of gas outburst in the coal seam of the working face, it is necessary to excavate the gas drainage roadway under the 2-1 coal seam. Multilayer aquifers generally exist under coal seam 2-1, as shown in Figure 6. The floor aquifer nearest of 2-1 coal seam is L9 limestone and L8 limestone. The L9 limestone has a small water storage capacity due to its thin rock strata, so the water inrush danger has been relieved by means of draining. The L8 limestone rock strata are thick and rich in water, with a water pressure of 3.24 MPa to 6.84 MPa, which is the principal water-filled aquifer that seriously threatens the floor roadway. Once confined water in the underlying confined aquifer breaks through the barrier of the floor rock, it flows into the roadway along the water-conducting fissure zone of the floor, which will cause the occurrence of floor water inrush accidents. Therefore, the floor roadway faces heavy water inrush hazards during the excavation and the entire service cycle.

3.2. Numerical Simulation Model. According to the geological conditions of the floor roadway in Zhaogu No. 2 Coal Mine, the expansion characteristics of the surrounding rock plastic zone of the floor roadway under different stress environments are analyzed through FLAC^{3D} numerical simulation. A model with length × width × height = 500 m × 1 m × 50 m is established, as shown in Figure 7. The floor roadway is located in the middle of the model and is a straight wall semicircular arch with width × height = 5.0 m × 4.0 m. The thickness of each rock strata in the model adopts the actual geological thickness, and the lithology of the coal seam adopts the same lithology as the basic roof to avoid affecting the simulation effect. The stratum layout and rock mechanics parameters used in the model are shown in Table 1. The model adopts the Mohr-Coulomb constitutive model, which fixes the horizontal displacement of the x- and y-axis boundary and the vertical displacement of the lower boundary of the z-axis. The pore water pressure $P_W = 4$ MPa is applied in the range of L8 limestone to simulate the water pressure of the aquifer, the compensation load 17.75 MPa is applied to the upper boundary, and the fixed initial stress $P_Z = 17.75$ MPa. By changing the size of P_X and P_Y the failure zone of the floor roadway, surrounding rock under different stress ratio is simulated.

3.3. Numerical Simulation Results. Figure 8 shows the distribution results of the plastic zone in the surrounding rock of floor roadway under different stress ratio conditions. It can be observed that when $\lambda = 1$, the plastic zone of the roadway surrounding rock is more evenly distributed among the roof and two sides of the roadway. Because the lithology of the floor is harder, the plastic failure range is smaller. When $\lambda = 2$, the plastic zone of the surrounding rock of the roadway has a relatively obvious expansion, and the contours of the plastic zone in the roof and the two sides are approximately elliptical. The range of the plastic zone in the floor has also increased significantly, but its distribution range is not as large as that of the two sides and the roof. When $\lambda = 2.5$, the size of the plastic zone of the surrounding rock continues to increase, and the "butterfly" nonuniform expansion characteristics of the plastic zone appear in the direction of the shoulder angle of the roof and the bottom angle of the floor. However, because of the strong lithology in the floor, the "butterfly" condition has not been reached, so the plastic zone of the surrounding rock in the floor does not show the characteristics of nonuniform expansion. When $\lambda = 3$, it can be seen that the "butterfly" plastic zone of the roof and the two sides has a relatively obvious increase and it begins to expand in the direction of 45° on both sides. The plastic zone in the bottom plate also began to show the nonuniform distribution of "butterfly" in the mudstone stratum in the basic bottom, and the direction of the butterfly leaf was 45° obliquely downward. At this time, the stress conditions began to be slightly changed. When λ increased to 3.1, the plastic zone of the roof of the roadway increased significantly, and the plastic zone of the floor also showed noticeable "butterfly" distribution characteristics. When λ continues to increase to 3.2, although the stress conditions are only minimal changed, the range of its plastic zone has shown a very obvious malignant expansion. At this time, the plastic zone of the roof surrounding rock of the roadway is directly connected to the roof coal seam, and the plastic zone of the surrounding rock of the roadway floor is also connected with the L8 limestone below. The plastic zone generated by the surrounding rock of the floor roadway will form a water channel, so that the L8 limestone can reach the floor roadway and the coal seam floor through the plastic zone of the floor roadway surrounding rock.

Numerical simulation analysis shows that the plastic failure range of the floor roadway surrounding rock is relatively small under the environment of small lateral pressure coefficient. When the plastic zone begins to show a butterfly shape, with the increase of the lateral pressure coefficient, the plastic failure range begins to increase significantly. When the lateral pressure coefficient is large, a minimal change in stress conditions will cause the malignant expansion of the plastic zone of the roadway surrounding rock. When the plastic damage range of the surrounding rock is large enough to communicate with the floor aquifer, the floor water will flow into the floor roadway along the channel created by the damaged rock mass. At this time, the plastic fracture of the floor roadway will cause the cracks in the rock mass to become water channels, providing necessary conditions for water inrush from the coal floor and roadway.

4. Butterfly Water Inrush Mechanism in Roadway

4.1. Risk Analysis of Water Inrush in Roadway. Usually the floor water inrush needs to meet the following conditions:

Bore histogram	Lithology	Thickness (m)	Remarks
	2-1 Coal seam	6.12	Black, with submetallic luster, massive, containing a small amount of powder, coal seam structure is simple, some contain a layer of gangue.
Aquiclude	Mudstone	7.54	Dark gray, with horizontal bedding, with siderite mudstone, fracture development and calcite filling.
Aquiclude	Sandy mudstone	7.46~9.73	Argillaceous cementation, the occurrence of rock strata is stable, and there are small changes in some parts.
Permeable layer	L9 limestone	1.5~1.9	Dark gray, with some fusulinidae fossils and developed fissures filled with calcite veins.
Aquiclude	Mudstone	4.7	Dark gray, with thin siderite mudstone in the upper part, brittle and hard.
Aquiclude	Sandy mudstone	4.8	Gray black and contains a small amount of muscovite. There is a layer of siderite mudstone in the middle and lower part, and the fractures are filled with calcite.
Aquifer	L8 limestone	6.8~10.11	Dark gray, aphanitic texture, local fissures and calcite veins, with star like pyrite.

Figure 6: The comprehensive histogram of rock strata in coal seam.

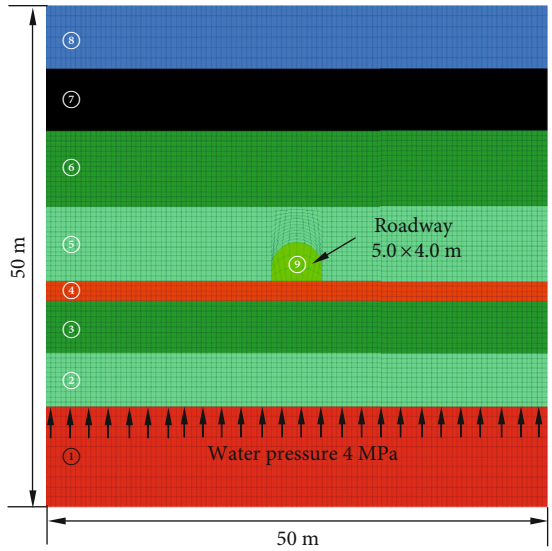

Figure 7: The numerical stress model of floor roadway in nonuniform stress field under the influence of water pressure.

first, there is an underlying confined aquifer; second, the aquifer has strong water-rich; then, the confined aquifer has sufficient head pressure; finally, there are water channels between the aquifer and the production space. The first three conditions exist objectively with the geological conditions of the coal seam, and the water channel can be produced by natural existence and mining disturbance. Therefore, under certain geological conditions, the key to preventing water inrush from the floor is to ensure the water resistance of the floor rock to the greatest extent and to prevent the generation of water channels.

The floor roadway of the 11060 working face of Zhaogu No. 2 Coal Mine is arranged under the working face, as shown in Figure 9. To minimize the risk of water inrush between the working face and the floor roadway, it is necessary to ensure that the floor has a thickness of the water barrier sufficient to resist the head pressure of the bottom aquifer. Under the influence of mining, the surrounding rock of the floor roadway will inevitably produce a certain degree of damage to reduce the thickness of the original floor water barrier. The thickness of the floor safety water barrier can be expressed as follows:

$$H_S = (h_1\text{-}h_3)\text{-}(h_2\text{-}h_3) = h_1\text{-}h_2, \quad (2)$$

where H_s is the safety water-proof thickness, h_1 is the thickness of undamaged rock stratum, h_2 is the thickness of the floor roadway surrounding rock failure zone, and h_3 is the thickness of permeable layer, $h_3 \subseteq h_2$.

Due to the small thickness of L9 limestone and poor water-bearing, it has been drained to eliminate the danger of water inrush, so it is only considered a permeable layer here. And the thickness of the floor safety water-proof layer is the difference between the total thickness of floor layer and the failure thickness. The size of h_1 and h_2 are determined by the thickness of the floor aquiclude and the permeable layer, the height of the confined water uplift zone, the floor failure depth of the goaf, and the failure thickness of the floor roadway surrounding rock. Under the corresponding geological conditions, the thickness of the floor water-proof layer, the thickness of the permeable layer, and the height of the confined water-conducting zone will be determined. The floor damage depth of the goaf is closely related to the mining method of the working face. These factors have a stable impact on the thickness of the floor safety water-proof layer relatively. The damage range of the surrounding

Table 1: Model layout and rock mechanics parameters.

Number	Stratum name	Thickness (m)	ρ (kg·m^{-3})	K (GPa)	G (GPa)	φ (°)	c (MPa)	R_m (MPa)
⑨	Roadway	—	2500	10.44	4.54	28	3.36	2.60
⑧	Main roof	6.3	2200	8.82	5.04	33	5.56	1.48
⑦	2-1 coal seam	6.2	2200	8.82	5.04	33	5.56	1.48
⑥	Mudstone	7.5	2200	8.82	5.04	30	3.24	1.48
⑤	Sandy mudstone	7.5	2500	10.44	4.54	28	3.36	2.60
④	L_9 limestone	2	2700	12.6	8.3	40	10	8.71
③	Mudstone	5.2	2200	8.82	5.04	30	3.24	1.48
②	Sandy mudstone	5.3	2500	10.44	4.54	28	3.36	2.60
①	L_8 limestone	10	2700	12.6	8.3	40	10	8.71

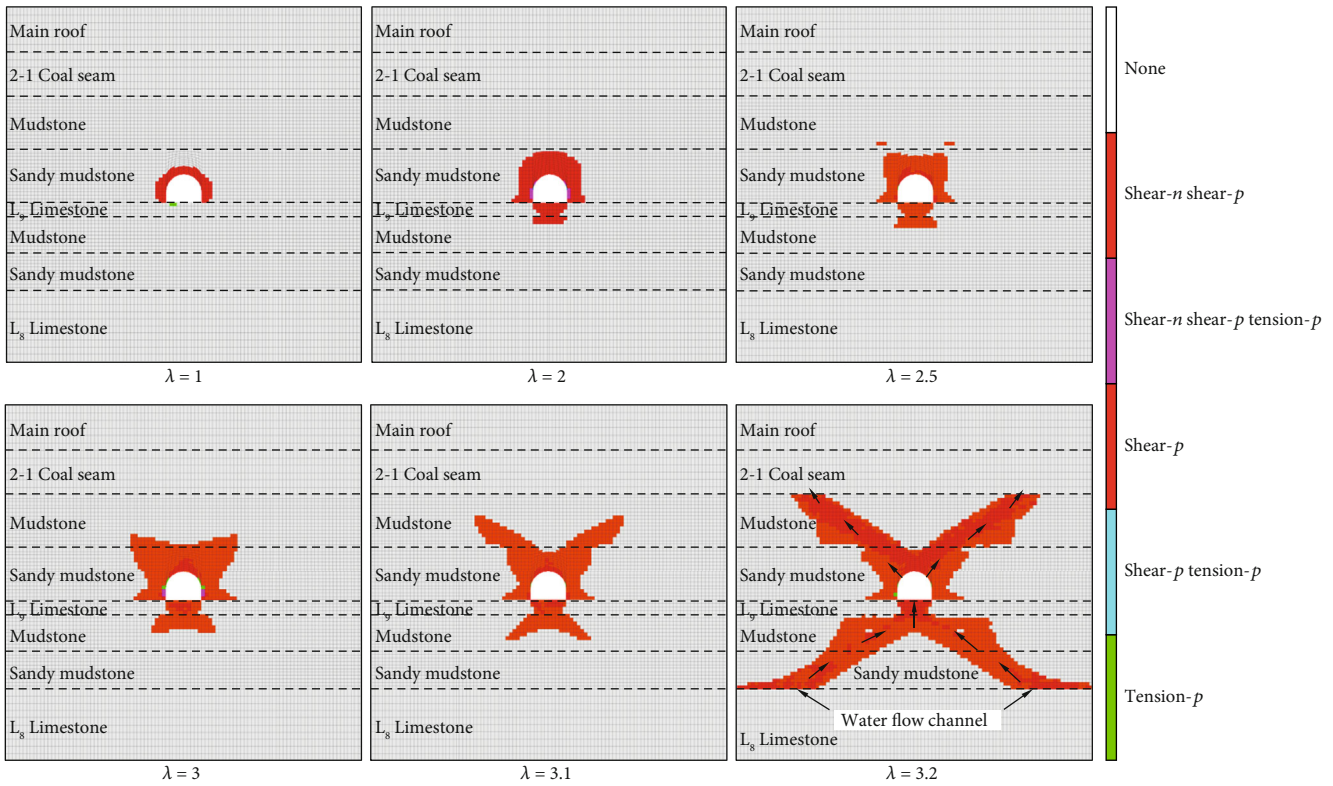

Figure 8: The numerical simulation result of butterfly-shaped plastic zone.

rock of the floor roadway is different under different stress environments, which plays a key role in the thickness of the floor safety water-proof layer; that is, the damage range of the floor roadway surrounding rock directly affects the thickness of the floor safety water-proof.

The main factor that affects the risk of water inrush from the floor is the thickness of the safety water-proof layer. The greater the thickness of the safety water-proof layer, the lower the risk of water inrush. Under the influence of mining stress, the surrounding rock of the roadway will produce a certain range of damage zone, which will damage the water-resistant rock layer near the floor roadway and affect its water resistance. The greater the damage range of the roadway surrounding rock, the greater the impact on the water-resistant layer of the coal floor. For floor roadways, a certain thickness of safety water-proof layer under the floor roadway is required to resist water pressure, so the floor damage range caused by the surrounding rock of the floor roadway will directly affect the thickness of the floor safety water-proof layer.

4.2. Butterfly Water Inrush Mechanism in Roadway. In floor roadway engineering, the surrounding rock of the roadway will produce a certain degree of damage zone under the action of stress. When the damage zone is in the aquiclude, it will affect the thickness of the safe water-proof. In nonuniform stress field, the roadway surrounding rock will appear butterfly plastic zone, which is highly sensitive to stress. Small changes in stress will lead to severe expansion of

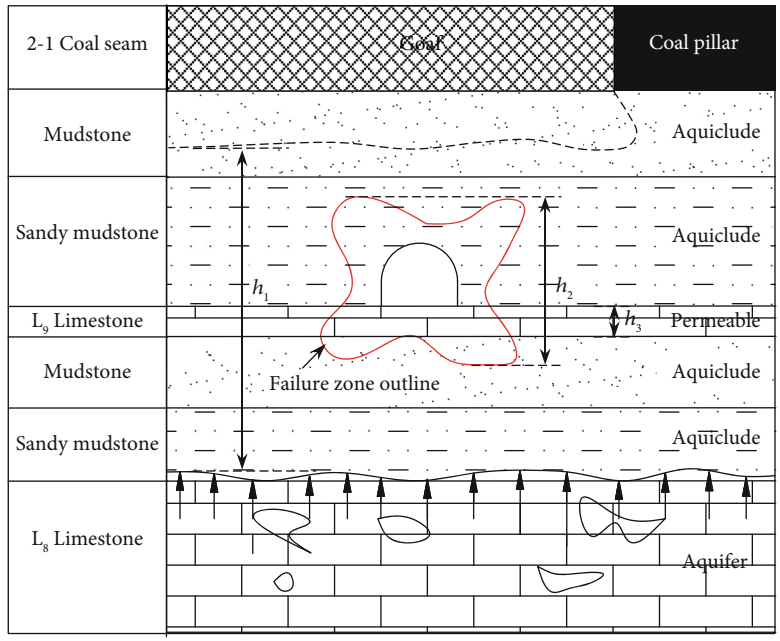

Figure 9: The influence of surrounding rock disturbance on the thickness of aquifers.

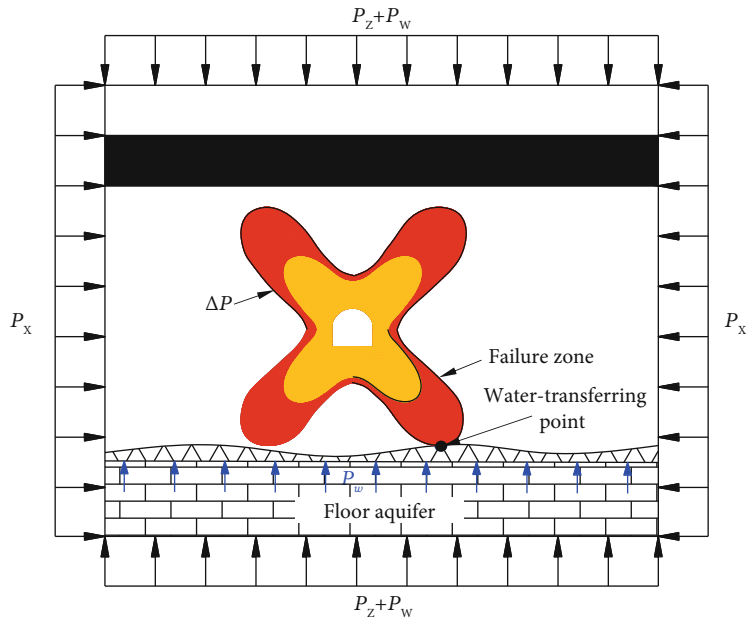

Figure 10: The schematic of "butterfly-shaped water inrush" of the floor roadway.

butterfly-shaped plastic zone. When large butterfly damage zone occurs to the surrounding rock of the floor roadway, it is very easy to communicate with the L8 aquifer below, forming a confined water flowing into the floor roadway and coal seam floor, leading to water inrush accidents.

Under the environment of a large biaxial stress ratio, when the failure characteristics of the surrounding rock of the floor roadway show a "butterfly" shape, a small stress change will cause the plastic zone to expand malignantly. When the failure zone and the water transferring point are connected, the floor water will enter the damaged rock body through the water transferring point, and eventually flow into the roadway space, causing a water inrush accident. Therefore, the uneven and malignant expansion of the plastic zone only occurs when the plastic zone presents a "butterfly" feature, and the necessary water channel for water inrush can be formed. Therefore, this kind of water inrush caused by butterfly expansion of surrounding rock failure in floor roadway is called butterfly water inrush, as shown in Figure 10. The necessary condition for "butterfly water inrush" is the existence of a large biaxial stress ratio environment in the surrounding rock.

5. Conclusions

In order to reveal the mechanism of the roadway water inrush above confined water, we established the force model of the roadway surrounding rock above confined water in nonuniform stress field and studied the shape characteristics and expansion law of the roadway surrounding rock plastic zone. Based on the work presented in this paper, the following conclusions are made:

(1) Under different lateral pressure coefficient, the roadway surrounding rock will form different shapes of plastic zone. When $\lambda = 1$, the roadway surrounding rock plastic zone is circular; with the increase of lateral pressure coefficient, the shape of plastic zone changes from circular to elliptical; when $\lambda > 2$ or $\lambda < 0.5$, the shape of plastic zone becomes butterfly

(2) When the shape of the roadway plastic zone is circular or elliptic, the maximum radius increases linearly with the increase of regional stress. When the shape is butterfly, the maximum radius increases exponentially with the increase of stress, and the maximum radius of plastic zone tends to infinity when the stress level reaches a certain limit value

(3) The water inrush mechanism of roadway above the aquifer in nonuniform stress field is revealed. Under the condition of larger bidirectional stress ratio, the roadway surrounding rock will show butterfly-shaped failure, and small stress change will cause malignant expansion of the plastic zone; when the plastic failure zone is connected with the underlying aquifer, confined water of floor will enter the rock mass from the water diversion point and eventually flood into the roadway, causing floor water inrush

Data Availability

The data used to support the findings of this study are available from the corresponding author upon request.

Conflicts of Interest

The authors declare no conflict of interest.

Acknowledgments

The authors wish to sincerely thank various organizations for their financial support. This work was partially supported by the National Natural Science Foundation of China (Grant no. 52004289) and the National Key Research and Development Program (Grant no. 2016YFC0600708).

References

[1] Q. Wu, Y. Du, H. Xu, Y. Zhao, X. Zhang, and Y. Yao, "Finding the earliest arrival path through a time-varying network for evacuation planning of mine water inrush," *Safety Science*, vol. 130, pp. 1–9, 2020.

[2] H. Jiang, L. Li, X. Rong, M. Y. Wang, Y. P. Xia, and Z. C. Zhang, "Model test to investigate waterproof-resistant slab minimum safety thickness for water inrush geohazards," *Tunnelling and Underground Space Technology*, vol. 62, pp. 35–42, 2017.

[3] L. Li, S. Li, and Q. Zhang, "Study of mechanism of water inrush induced by hydraulic fracturing in karst tunnels," *Rock and Soil Mechanics*, vol. 31, pp. 523–528, 2010.

[4] L. Shi, M. Qiu, Y. Wang, X. Qu, and T. Liu, "Evaluation of water inrush from underlying aquifers by using a modified water-inrush coefficient model and water-inrush index model: a case study in Feicheng coalfield, China," *Hydrogeology Journal*, vol. 27, no. 6, pp. 2105–2119, 2019.

[5] S. Li, X. Li, and H. Ding, "Research development of catastrophe mechanism and forecast controlling theory of water inrush and mud gushing in deep long tunnel," *China Basic Science*, vol. 19, pp. 27–43, 2017.

[6] S. Li, L. Li, and S. Li, "Development and application of similar physical model test system for water inrush of underground engineering," *Journal of Mining & Safety Engineering*, vol. 27, pp. 299–304, 2010.

[7] D. Liu, Z. Gu, R. Liang et al., "Impacts of pore-throat system on fractal characterization of tight sandstones," *Geofluids*, vol. 2020, Article ID 4941501, 17 pages, 2020.

[8] J. Wang, Y. Zhang, Z. Qin, S. Song, and P. Lin, "Analysis method of water inrush for tunnels with damaged water-resisting rock mass based on finite element method-smooth particle hydrodynamics coupling," *Computers and Geotechnics*, vol. 126, pp. 1–10, 2020.

[9] J. Chen, J. Zhao, S. Zhang, Y. Zhang, F. Yang, and M. Li, "An experimental and analytical research on the evolution of mining cracks in deep floor rock mass," *Pure and Applied Geophysics*, vol. 177, no. 11, pp. 5325–5348, 2020.

[10] K. Peng, H. Lv, Q. Zou, Z. Wen, and Y. Zhang, "Evolutionary characteristics of mode-I fracture toughness and fracture energy in granite from different burial depths under high-temperature effect," *Engineering Fracture Mechanics*, vol. 239, article 107306, 2020.

[11] S. Liu, W. Liu, and D. Yin, "Numerical simulation of the lagging water inrush process from insidious fault in coal seam floor," *Geotechnical & Geological Engineering*, vol. 35, no. 3, pp. 1013–1021, 2017.

[12] J. Cheng, X. Sun, Z. Gong, G. Feng, and Z. Jian, "Numerical simulations of water-inrush induced by fault activation during deep coal mining based on fluid-solid coupling interaction," *Disaster Advances*, vol. 6, pp. 10–14, 2013.

[13] Q. Wu, Y. Liu, and Y. Liu, "Using the vulnerable index method to assess the likelihood of a water inrush through the floor of a multi-seam coal mine in China," *Mine Water & the Environment*, vol. 30, pp. 54–60, 2011.

[14] Q. Wu, Y. Liu, D. Liu, and W. Zhou, "Prediction of floor water inrush:the application of GIS-based AHP vulnerable index method to Donghuantuo coal mine, China," *Rock Mechanics and Rock Engineering*, vol. 44, no. 5, pp. 591–600, 2011.

[15] Q. Wu, D. Zhao, Y. Wang, J. Shen, and H. Liu, "Method for assessing coal-floor water-inrush risk based on the variable-weight model and unascertained measure theory," *Hydrogeology Journal*, vol. 25, pp. 1–15, 2017.

[16] Y. Zhao, Y. Wang, W. Wang, L. Tang, Q. Liu, and G. Cheng, "Modeling of rheological fracture behavior of rock cracks

subjected to hydraulic pressure and far field stresses," *Theoretical and Applied Fracture Mechanics*, vol. 101, pp. 59–66, 2019.

[17] Y. Zhao, L. Zhang, J. Liao, W. Wang, Q. Liu, and L. Tang, "Experimental study of fracture toughness and subcritical crack growth of three rocks under different environments," *International Journal of Geomechanics*, vol. 20, no. 8, p. 04020128, 2020.

[18] Y. L. Zhao, L. Y. Zhang, W. J. Wang, Q. Liu, L. M. Tang, and G. Cheng, "Experimental study on shear behavior and a revised shear strength model for infilled rock joints," *International Journal of Geomechanics*, vol. 20, article 04020141, 2020.

[19] Y. L. Zhao, C. S. Zhang, Y. X. Wang, and H. Lin, "Shear-related roughness classification and strength model of natural rock joint based on fuzzy comprehensive evaluation," *International Journal of Rock Mechanics and Mining Sciences*, vol. 137, 2020.

[20] W. Yin, "Analysis on water inrush factors of working face floor and control measures," *Coal Geology of China*, vol. 9, pp. 44–47, 1997.

[21] Y. Zhao, P. F. He, Y. F. Zhang, and L. Wang, "A new criterion for a toughness-dominated hydraulic fracture crossing a natural frictional interface," *Rock Mechanics and Rock Engineering*, vol. 52, no. 8, pp. 2617–2629, 2019.

[22] Y. Zhao, C. L. Wang, Y. F. Zhang, and Q. Liu, "Experimental study of adsorption effects on shale permeability," *Natural Resources Research*, vol. 28, no. 4, pp. 1575–1586, 2019.

[23] Y. Zhao, C. L. Wang, and J. Bi, "Analysis of fractured rock permeability evolution under unloading conditions by the model of elastoplastic contact between rough surfaces," *Rock Mechanics and Rock Engineering*, vol. 53, no. 12, pp. 5795–5808, 2020.

[24] H. Kang, X. Zhang, L. Si, Y. Wu, and F. Gao, "In-situ stress measurements and stress distribution characteristics in underground coal mines in China," *Engineering Geology*, vol. 116, no. 3-4, pp. 333–345, 2010.

[25] L. Jiang, A. Sainoki, H. S. Mitri, N. Ma, H. Liu, and Z. Hao, "Influence of fracture-induced weakening on coal mine gateroad stability," *International Journal of Rock Mechanics and Mining Sciences*, vol. 88, pp. 307–317, 2016.

[26] G. Zhang, L. Chen, Z. Wen et al., "Squeezing failure behavior of roof-coal masses in a gob-side entry driven under unstable overlying strata," *Energy Science & Engineering*, vol. 8, no. 7, pp. 2443–2456, 2020.

[27] X. Guo, Z. Zhao, X. Gao, X. Wu, and N. Ma, "Analytical solutions for characteristic radii of circular roadway surrounding rock plastic zone and their application," *International Journal of Mining Science and Technology*, vol. 29, no. 2, pp. 263–272, 2019.

[28] Z. Tao, Z. Song, M. He, Z. Meng, and S. Pang, "Principles of the roof cut short-arm beam mining method (110 method) and its mining-induced stress distribution," *International Journal of Mining Science and Technology*, vol. 28, no. 3, pp. 391–396, 2018.

[29] Y. Li, N. Ma, and J. Ma, "Surrounding rock's failure characteristic and rational location of floor gas drainage roadway above deep confined water," *Journal of China Coal Society*, vol. 43, pp. 2491–2500, 2018.

[30] L. Jiang, Y. Zhao, N. Golsanami, L. Chen, and W. Yan, "A novel type of neural networks for feature engineering of geological data: case studies of coal and gas hydrate-bearing sediments," *Geoscience Frontiers*, vol. 11, no. 5, pp. 1511–1531, 2020.